RSC Advances

PAPER

Cite this: *RSC Adv.*, 2016, **6**, 71507

Flame synthesis of nitrogen doped carbon for the oxygen reduction reaction and non-enzymatic methyl parathion sensor

Natarajan Karikalan,[a] Murugan Velmurugan,[a] Shen-Ming Chen,*[a] Chelladurai Karuppiah,[ab] K. M. Al-Anazi,[c] M. Ajmal Ali[d] and Bih-Show Lou*[ef]

Received 19th April 2016
Accepted 29th June 2016

DOI: 10.1039/c6ra10130e

www.rsc.org/advances

Growing concerns about the economical feasibility of materials synthesis means that simple methodologies to furnish materials are needed. Moreover, the multi-functional activity of these as-prepared materials is of great importance. Hence, here we report nitrogen-doped carbon nanoparticles from a one-step flame synthesis by directly burning pyrrole at room temperature and in an air atmosphere. The as-synthesized N-doped carbon was scrutinized as a cathode material for the oxygen reduction reaction and was also demonstrated in an electrochemical sensor. Furthermore, X-ray photoelectron spectroscopy (XPS) and Raman analysis was carried out to confirm the percentage of nitrogen content, the bonding environment and the disorder of carbon. The as-prepared N-doped carbon exhibits superior electrocatalytic activity towards the ORR compared with a commercial Pt/C catalyst. Moreover, the N-doped carbon modified glassy carbon electrode manifests a sensitive electrochemical response towards the detection of methyl parathion. A linear response was demonstrated by the fabricated sensor across two concentration ranges, from 0.0025 to 1 μM and 1 to 100 μM, with a lower detection limit of 0.068 nM. The proposed method is very simple, low cost and it can be utilized for practical applications to produce carbon materials on a large scale.

1. Introduction

The increasing demand of energy and anthropogenic climate change has induced a need for green energy and also environmental security.[1] Fuel cells are devices which generate electricity by the electrochemical transformation of hydrogen and oxygen into water.[2] They produce energy in a greener way, however, the fuel cells suffer from the sluggish oxygen reduction reaction (ORR) at the cathode side.[3] So far, platinum or platinum based compounds have mostly been employed as ORR catalysts due to their superior activity and stability.[4] However, the use of platinum for fuel cell application has declined due to its high cost and relatively low abundance. Hence, recent studies have pursued non-precious metals and metal-free catalysts for the ORR.[5–8] The non-noble metal catalysts have revealed a better performance towards the ORR, though, they are used with carbonaceous support materials,[9–11] because non-precious metal catalysts generally have a lower surface area and poor electrical conductivity, and hence the carbons are used to reimburse the conductivity. Recent studies have exhibited carbon materials solely engaged in the ORR, which are so-called metal-free catalysts.[12–14] In particular, the N-doped graphene materials have revealed excellent electrocatalytic responses towards the ORR.[15]

On the other hand, to secure the environmental safety, it is necessary to remove organic pollutants, mainly carcinogenic and lethal hazardous compounds,[16] especially pesticides, which are extensively used in agriculture to control insects.[17] Methyl parathion (MP-organophosphorous compound) is one of the most commonly used pesticides around the world; however, it contaminates soil and water bodies which affects the aquatic organisms.[17] Hence, it is very important to develop a viable method to detect MP in water, foodstuff and soils, *etc.* Several analytical techniques have been employed to determine the level of MP, such as gas chromatography (GC), high performance liquid chromatography (HPLC), gas chromatography-mass spectrometry (GC-MS) and spectrometry.[18–20] These methods manifest accurate results with high sensitivity;

[a]*Electroanalysis and Bioelectrochemistry Lab, Department of Chemical Engineering and Biotechnology, National Taipei University of Technology, No. 1, Section 3, Chung-Hsiao East Road, Taipei 106, Taiwan, Republic of China. E-mail: smchen78@ms15.hinet.net*

[b]*Department of Chemistry, National Taiwan University, No. 1, Section 4, Roosevelt Road, Taipei 106, Taiwan, Republic of China*

[c]*Department of Zoology, College of Science, King Saud University, Riyadh-11451, Saudi Arabia*

[d]*Department of Botany and Microbiology, College of Science, King Saud University, Riyadh-11451, Saudi Arabia*

[e]*Chemistry Division, Center for General Education, Chang Gung University, Taoyuan, Taiwan, Republic of China. E-mail: blou@mail.cgu.edu.tw*

[f]*Department of Nuclear Medicine and Molecular Imaging Center, Chang Gung Memorial Hospital, Taoyuan, Taiwan, Republic of China*

however, they are time consuming processes and very expensive for practical applications. Therefore, a rapid, selective and sensitive method is still needed for the detection of MP. Incidentally, an electrochemical technique offers an alternative and cost effective way to detect MP compared to the former methods.[21] Here, graphene or composites of graphene are also used to fabricate the sensor electrode.

Since the discovery of graphene, a vast number of studies have been devoted to scrutinize the properties of graphene-based nanomaterials and its composites towards numerous electrochemical applications.[22] Graphene has given an advanced platform to modern research due to its remarkable properties and versatility.[23] However, the synthesis of graphene or graphene based materials is lacking by the limitations in the synthetic procedures, such as the mechanical exfoliation of graphite, thermal exfoliation of graphite, chemical vapor deposition on silicon wafers and the reduction of graphene oxide (GO).[24–26] So far, the identified methods are significantly costly or questionable in terms of their safety; hence, the adaptability of graphene synthesis should be improved for practical applications. Therefore, recent studies have concentrated on activated carbons (ACs) because of their simple synthesis processes, safety and economic viability.

ACs are synthesized from many sources (*e.g.*, biomass, organic chemicals and charcoal) and are widely used as adsorption materials due to their high porosity and high surface area. Nowadays, they are employed in heterogeneous catalysis and electrocatalysis, particularly in energy and environmental applications.[27–30] Moreover, heteroatom (boron, nitrogen, phosphorous and sulfur) doped carbons exhibit excellent electrocatalytic activity when compared with undoped carbons.[12–15,31] Of these heteroatom doped carbons, nitrogen doped carbons have acquired tremendous interest in the fields of ORR and sensors.[7,8,15] Among the various methods, flame syntheses are able to furnish carbon materials in a simple and very rapid single step.[32] This method has attracted great interest and is motivated from the recently reported candle soot synthesis procedure.[33,34] Herein, we report the synthesis of nitrogen doped carbon nanoparticles (NCN) from the direct burning of pyrrole in an air atmosphere and the resultant carbon soot was deposited on a glass plate. Furthermore, the as-prepared nitrogen doped carbon nanoparticles were characterized by various physical characterization and electrochemical characterization towards the detection of MP and in the ORR.

2. Experimental section

2.1. Preparation and fabrication of nitrogen doped carbon-modified electrode

The previously reported flame synthesis method was followed with some modifications to synthesise nitrogen doped carbon in the form of soot.[32] Herein, 10 mL of pyrrole was taken in a small beaker and directly burned under air. Obviously, the aromatic organic compounds burned with a sooty flame when igniting, and afterwards the resultant soot was deposited on a glass plate and the sample was carefully collected by scratching. In addition, the synthesis procedure was given as a schematic diagram which is shown in Scheme 1.

To fabricate the electrode for the ORR and the MP sensor, the NCN (44 mg in 5 mL) was dissolved in DI water and further sonicated for 15 min. The homogeneous NCN solution (8 μL) was drop casted on the well-polished glassy carbon electrode (GCE) and rotating disk electrode (RDE) dried in an ambient condition. The NCN modified electrodes were successfully used to observe the electrochemical behavior towards MP detection and ORR activity.

2.2. Characterization of NCN

The structure and bonding environment of NCN was analyzed by X-ray diffraction pattern analysis (XRD), XPERT-PRO (PANalytical B.V., The Netherlands) with CuKα radiation ($\lambda = 1.5406$ Å) and Raman spectra (NT-MDT, NTEGRA SPECTRA). The surface morphology and elemental composition were studied by scanning electron microscopy (SEM) using a Hitachi S-3000 H microscope. Primary electrochemical reactions such as cyclic voltammetry and chronoamperometry were carried out in a CHI 1205B electrochemical analyzer (CH Instruments, USA). Electrocatalytic determination of methyl parathion was performed by differential pulse voltammetry (DPV) using a CHI 900 apparatus (CH Instruments, USA). The oxygen reduction reaction and the number of electron transfers associated with the ORR were analyzed by a rotating disk voltammogram AFMSRX (PINE instruments, USA). A conventional three electrode system was employed for the catalysis where the GCE was used as a working electrode (0.07 cm^2), platinum wire acted as an auxiliary electrode and Ag/AgCl/3 M KCl was used as a reference electrode.

3. Results and discussion

3.1. Characterization of structure and surface morphology of NCN

Fig. 1b shows the XRD pattern of NCN, which reveals a peak at 25.82° (2θ), corresponding to the (002) plane with an interlayer spacing of 0.344 nm along the *c*-axis, which is closely matched with the interlayer spacing of pristine graphite (0.34 nm).[35] This result indicates that the as-prepared NCN was crystallized in the hexagonal ordered unit cell. But the presence of hetero atoms such as nitrogen and oxygen moieties in the crystal lattice leads the NCN to have a smaller grain size and greater disorder. Therefore, Raman spectroscopy was employed to assess the disorder in NCN. Fig. 1d displays a Raman spectrum of NCN which possesses two broad bands at 1352 and 1594 cm^{-1}, the observed peaks correspond to the disordered (D) band and graphitic (G) band.[36,37] The ratio of the relative intensities for D and G bands provides information about the compound's crystallinity; a lower D/G ratio indicates better crystallinity. The lower D band intensity of NCN evidences the low distortion in the hexagonal lattice and also the D/G intensity ratio of NCN is 0.78, which is directly proportional to the amount of disorder of the carbon.[38]

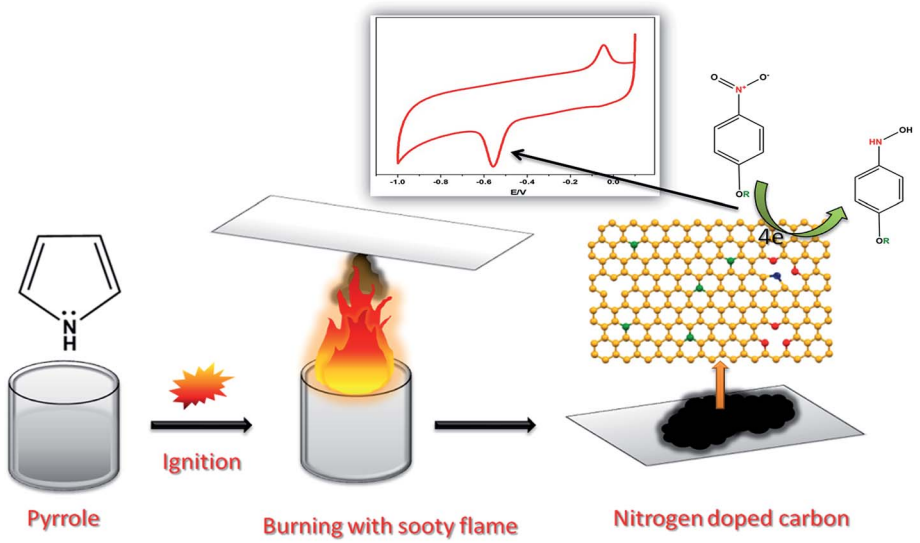

Scheme 1 A schematic representation of the synthesis of nitrogen doped carbon from pyrrole and its voltammetric response towards the detection of MP.

Fig. 2a displays the scanning electron microscopy (SEM) image of NCN, which shows an aggregated flake like surface morphology with an average elemental composition of 90.0, 7.1 and 2.9%, corresponding to C, O and N contents respectively (Fig. 2e). These relative atomic percentages for each element in NCN are further confirmed by the elemental mapping of energy dispersive X-ray analysis (EDAX), the results of which are shown in Fig. 2b–d. The local crystallinity and grain boundary of NCN was probed by transmission electron microscopy (TEM). Fig. 1c shows a TEM image of the as-prepared NCN, which depicts an

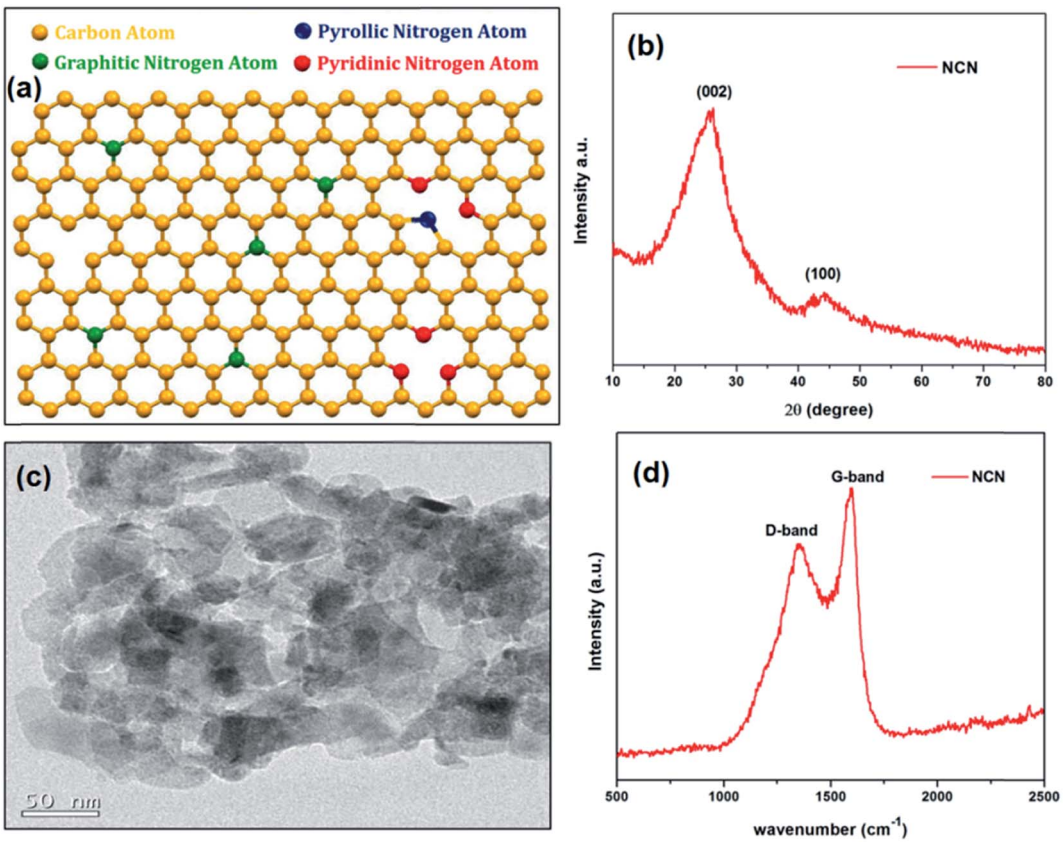

Fig. 1 (a) Crystal model, (b) XRD pattern, (c) TEM image and (d) Raman spectra of the as-prepared nitrogen doped carbon.

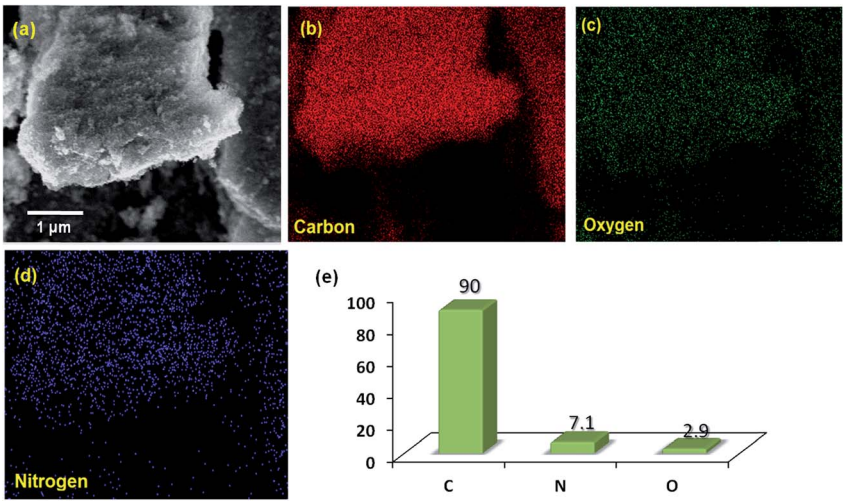

Fig. 2 (a) SEM image of NCN, (b–d) EDAX elemental mapping of NCN which illustrates the distribution of components, carbon (b) oxygen (c) and nitrogen (d). (e) Bar diagram of atomic percentage of each element of NCN.

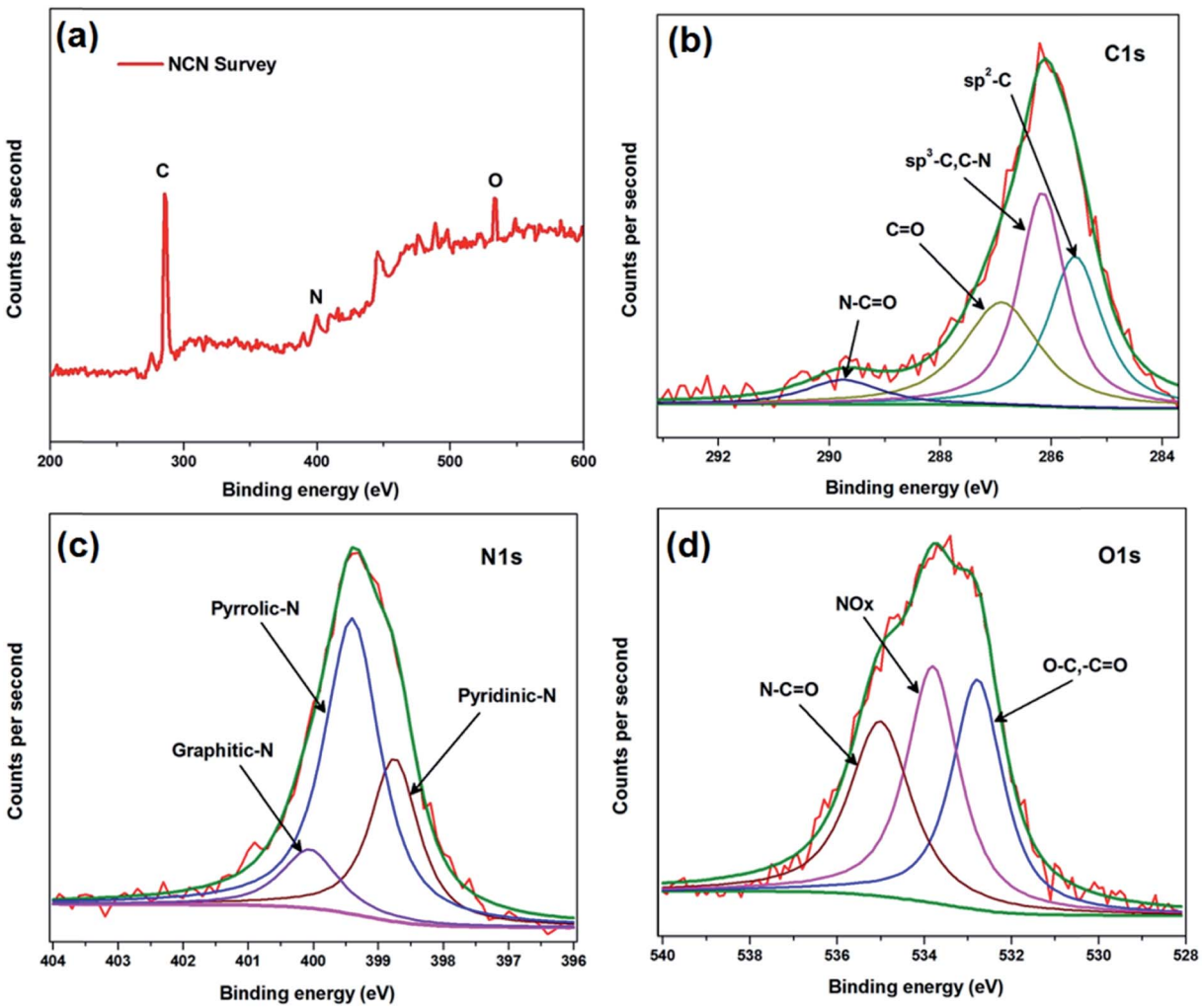

Fig. 3 (a) XPS survey of the as-prepared nitrogen doped carbon. High resolution XPS spectra with curve fitting for (b) C1s peak (c) N1s peak and (d) O1s peak.

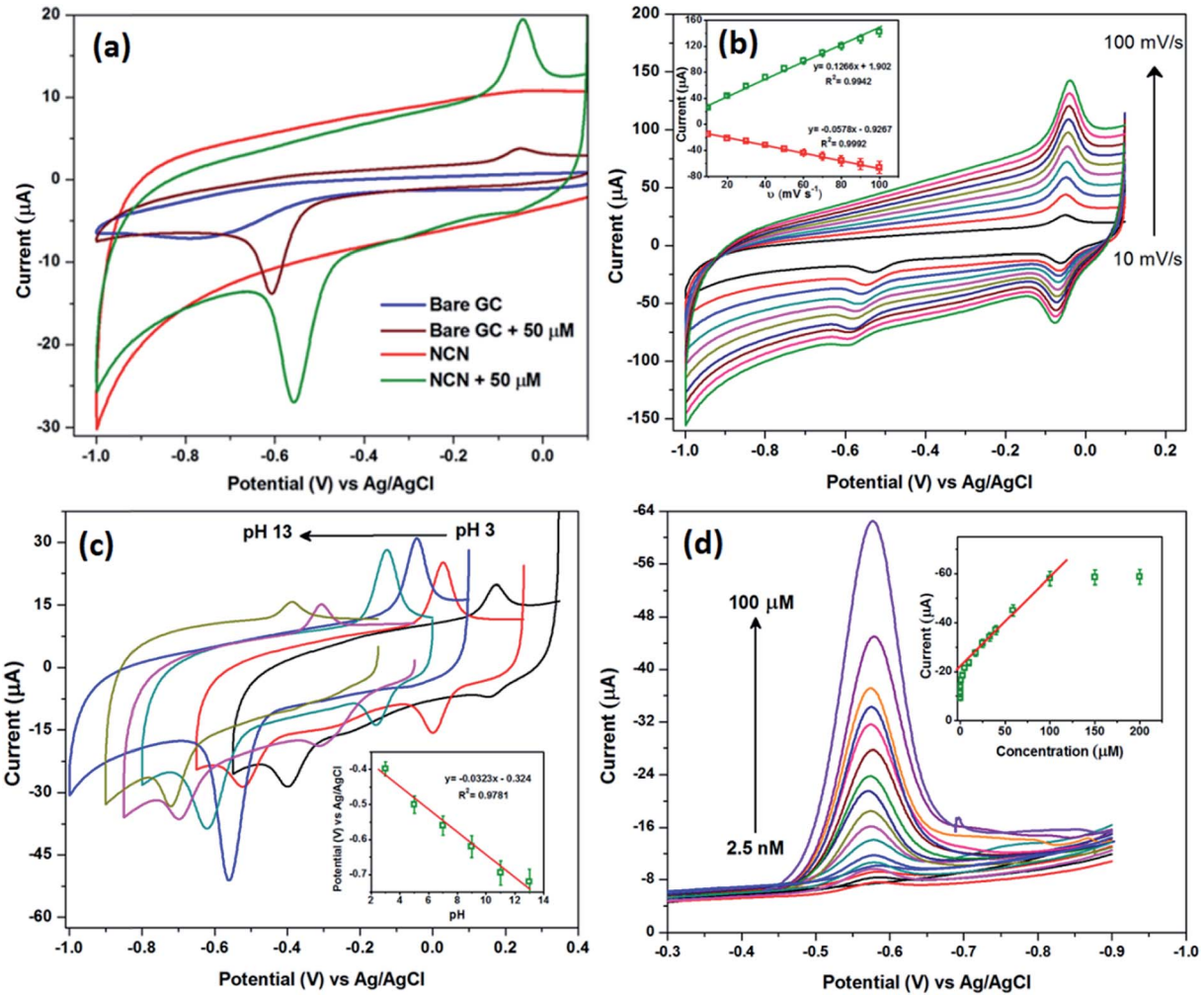

Fig. 4 Cyclic voltammograms of (a) bare and NCN modified GCE in presence and absence of 50 μM MP. (b) NCN modified GCE in MP at various scan rates ranging from 10 to 100 mV s^{-1} and the corresponding plot of peak current *vs.* scan rate in inset. (c) NCN modified GCE in MP at various pH values from 3 to 13, the inset shows the plot of pH *vs.* peak potential (taking the primary reduction peak). (d) Differential pulse voltammograms of NCN modified GCE in various concentrations of MP ranging from 2.5 nM to 100 μM and the inset shows the calibration plot of current *vs.* concentration.

aggregated particle like shape with distinguishable grain boundaries; however, in some places it covers the particles as sheets.

X-ray photoelectron spectroscopy (XPS) is a reliable tool used to analyze the elemental composition and bonding environment of the compounds. As depicted in Fig. 3a, the XPS survey of the NCN possesses three major peaks centered at 286.5, 399.5, and 533.8 eV, which correspond to C1s, N1s, and O1s, respectively. The relative elemental composition of the C1s, N1s, and O1s peaks is calculated from XPS as 89.5, 2.9, and 7.15%, respectively; this value is closely matched with the EDAX analysis. The high resolution N1s, O1s, and C1s spectra are considered to understand the bonding environment of the elements. Fig. 3b shows the high resolution spectra of C1s which further deconvoluted into four peaks; the peak at 285.5 eV is related to sp^2 carbon or graphitic carbon.

The peak at 286.1 eV is related to the sp^3 carbon where carbon bonds with nitrogen as C–N, or in other words, the graphitic nitrogen bond.[39] The peak at 286.9 eV is related to C=O, and the peak at 289.7 eV attributable to the N–C=O bond. This observation confirms the presence of nitrogen atoms in the carbon framework. Furthermore, a high resolution N1s spectrum was taken to account for a clear explanation. Fig. 3c depicts the N1s spectra of NCN, which contains three different bonding environments. The peaks at 398.73, 399.3, and 400.0 eV are assigned to pyridinic, pyrrolic, and graphitic nitrogen bonding. The crystal model of NCN is shown in Fig. 1a, which clearly illustrates information about the different environments of nitrogen in the carbon framework. The pyridinic and pyrrolic nitrogen atoms deviate the symmetry of C=C, and hence voids are created in the uniform carbon lattice. The high-resolution O1s spectra in Fig. 3d also shows evidence for the presence of nitrogen by the N–C=O bonding, which is in agreement with the C1s spectra. Oxygen was also doped in the carbon as C–O or –C=O, which is clearly observed by the peak at 532.7 eV. This

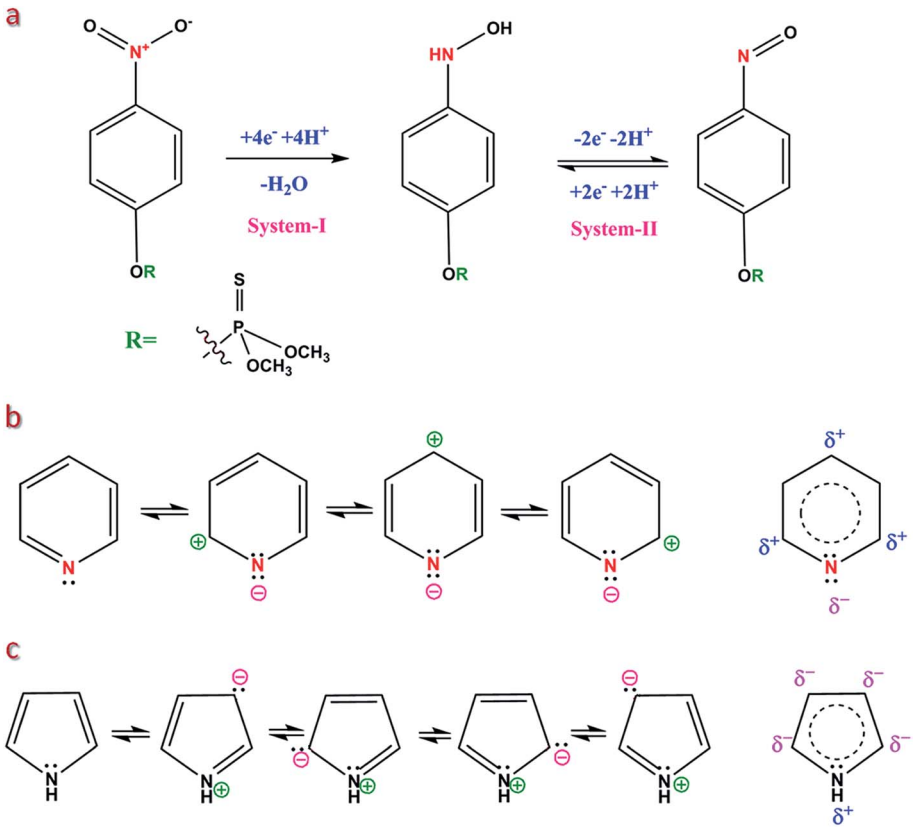

Scheme 2 (a) Plausible mechanism for the reduction of MP. (b & c) Delocalization of the electron clouds on the carbon atoms in pyridine and pyrrole.

may lead to good performance by increasing defects, disorder or the local electron density around the O atoms.

3.2. Electrochemical behavior of MP

To explain the mechanism of MP determination, cyclic voltammetry (CV) was used to characterize the electron transfer process concerning the reduction of MP. Fig. 4a shows the CVs obtained for the NCN modified and bare GCE in 0.1 M PBS (pH = 7.0) in the presence of 50 μM MP at a scan rate of 50 mV s^{-1}. These CVs were recorded only for the first cycles. In the cathodic sweep, a highly intense irreversible reduction peak (system-I, see Scheme 2a) was observed at −0.55 V for the NCN modified GCE, corresponding to the reduction of the nitro group in MP to arylhydroxylamine,[40] whereas bare GCE requires a 50 mV (−0.6 V) overpotential to reduce the MP. During the reverse scan, the primary reduced product (system-I, Scheme 2a) at the electrode surface was oxidized into nitrosobenzene (system-II, Scheme 2a) at −0.03 V; this oxidized product was further reduced in the second cathodic sweep at −0.06 V (see

Table 1 Comparison of the performance of NCN modified GCE towards the detection of methyl parathion with other previous reported works

Modified electrodes	Detection limit (nM)	Linear concentration range (μM)	References
Au/MWCNTs electrode	190	1.9–61	44
MWCNTs–chitosan/GCE	19	0.19–7.6	45
Silicate–CTAB/GCE	10	10–100	46
ZrO_2/CPE	7.6	0.019–11	47
OMC/GCE	7.6	0.09–61	48
pSC6–Ag NPs/GCE	4.0	0.01–80	49
MWCNTs–PAAM/GCE	2.0	0.005–10	50
GdHCF/GNs/GCE	1.0	0.008–10	51
Au ACs/Au	0.65	0.01–80	42
SH-CD/AuNPs/SWCNTs/GCE	0.1	0.002–0.08	52
ZnO/Ag/MPTMS/OHP	0.07	0.0025–75	53
NCN/GCE	0.068	0.0025–1, 1–100	Present work

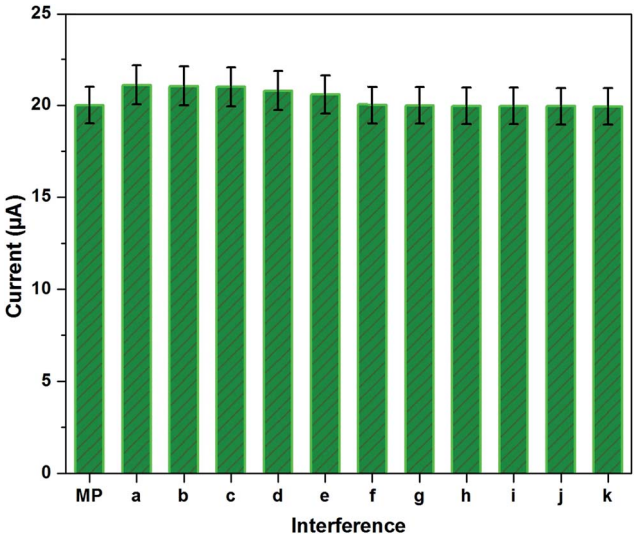

Fig. 5 Interference studies of NCN modified GCE in 0.1 M PBS containing MP in the presence of other potential interfering compounds, namely (a) paraoxon, (b) fenitrothion, (c) nitrobenzene, (d) *p*-nitrophenol, (e) nitroaniline, (f) Na^+, (g) K^+, (h) Ca^{2+}, (i) PO_4^{3-}, (j) NO_3^- and (k) Cl^- in concentrations of 10 and 100-fold excess with MP for (a–e) and (f–k) respectively.

scan rate).[41] For comparison, we also recorded a CV using the same electrodes in the absence of MP, it can be clearly seen that there were no peaks arising for the bare and NCN modified GCE (Fig. 4a). In addition, the obtained CV curves in the absence of MP provide information about the background current. Here, the bare GCE depicts reduction behavior at −0.75 *vs.* Ag/AgCl and provides low background current due to its low capacitance. On the other hand, NCN provides a high background current due to its superior high capacitance (due to the high surface to volume ratio).

3.3. Effect of scan rate and pH

The scan rate dependence of MP reduction was evaluated to assess the electron transfer process; hence, a range of different scan rates was used from 10 to 100 mV s^{-1}, and the resultant CVs are shown in Fig. 4b. It is well known that the reduction peak current increases systematically with increasing scan rate, but in our case the secondary redox product peak is observed better and is well shaped. This phenomenon indicates that the NCN modified GCE reduced a maximum of MP *via* a four electron pathway. Therefore, the secondary reduced product (system-I, Scheme 2a) remains a maximum at the electrode surface. Furthermore, a redox couple is produced (system-II, Scheme 2a). The peak current of the secondary product redox couple was plotted against the scan rate and is shown in Fig. 4b (inset). From the slope value in Fig. 4b (inset), we can find the redox process is diffusion controlled, however, the decrease in the primary reduction peak current indicates an adsorption process upon increasing the scan rate. Thus, the present study points out that the MP reduction was both an adsorption and diffusion controlled process, in which the adsorption occurs on the electrode surface and diffusion contributes to the rate determining step.[42] Moreover, the adsorption of MP onto the electrode surface was confirmed from the scan rate, where a small peak potential shift was observed in the MP reduction process with increasing scan rate.

The electrochemical reaction is very sensitive towards the pH of the electrolyte solution, where there is a linear response of the potential *versus* pH a slope of 59 mV (Nernst equation) for one electron transfer. The effect of pH on the electrocatalytic response of MP was evaluated for the NCN modified GCE in the pH range from 3 to 13. The NCN modified GCE exhibits the highest current response at a pH of 7.0 compared to all other pH values investigated (Fig. 4c). A decrease in current response was observed at a lower pH due to H^+ ion adsorption on the electrode surface. As shown in Fig. 4c (inset), the reduction peak potential of MP is linearly dependent on the pH in the range from 3 to 13. So, due to the electrocatalytic current enhancement, a pH value of 7.0 was selected for further experiments.

3.4. Determination of MP

Differential pulse voltammetry (DPV) is a more sensitive analytical method to determine the level of MP. This experiment was carried out to explore the practical viability of the NCN modified GCE for the non-enzymatic electrochemical detection of MP, a lethal environmentally hazardous pesticide. All DPV studies were recorded in 0.1 M PBS (pH = 7.0) by applying the potential window from −0.3 to −0.9 V with optimized pulse amplitude (0.05 V) and pulse width (0.05 s). Fig. 4d shows the DPV studies of the NCN modified GCE from a low concentration to a high concentration of MP, and it is obvious to see that when the concentration of MP is increased incrementally, the reduction current also increases systematically. It can be observed from Fig. 4d the reduction potential of MP shifts towards a more negative potential when the concentration is increased. This mainly arises from (i) the confined adsorption of the analyte (MP) on the NCN surface, or in other words, the formation of a thin film of analyte on the surface ahead of the diffusion layer, and (ii) a higher concentration of MP increases the solution resistance, and hence there is a tiny deviation in the ionic conductivity, which may shift the peak potential. Furthermore, the determination of MP was evaluated from the calibration plot of reduction current *vs.* the concentration of MP (Fig. 4d (inset)) where two linear curves were obtained over the concentration ranges of 0.0025–1 μM and 1–100 μM. Over these two linear concentration ranges, the sensitivity of the fabricated sensor was calculated as 72.4 nA μM^{-1} and 10 μA μM^{-1} respectively. The fabricated electrochemical sensor exhibits a low detection limit of 0.068 nM and presents a wide linear concentration range over the two different concentration ranges of MP. This study confirms that the proposed fabricated sensor effectively determined the MP concentration over a wide range of concentrations and displays a platform for practical applications. In order to evaluate the performance of the fabricated sensor, it was compared with previous reports. Comparisons are provided in Table 1.[44–53] A high linear concentration range and very low detection limit was observed for the fabricated sensor

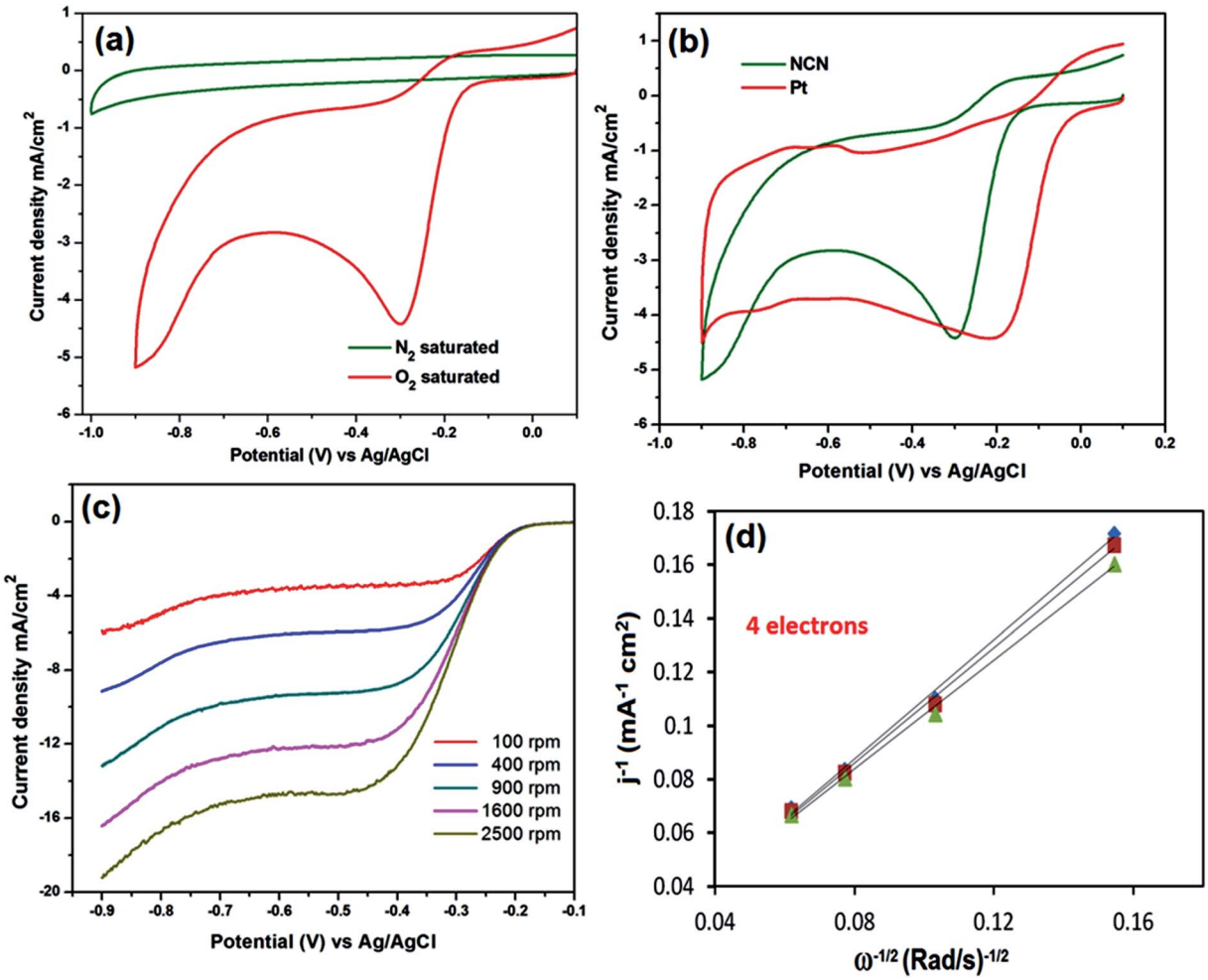

Fig. 6 Cyclic voltammograms of (a) NCN modified GCE in the presence of nitrogen and oxygen saturated 0.1 M NaOH. (b) Commercial Pt/C and NCN modified GCE in the presence of oxygen saturated 0.1 M NaOH. (c) RDE voltammograms of NCN modified GCE at various rotations. (d) KL-plot for the steady current obtained from the RDE voltammograms for NCN modified GCE.

when compared with previously reported materials. It can be seen that from the above studies, the NCN modified GCE manifests superior electrocatalytic performance towards the determination of MP.

3.5. Interference studies

To examine the selectivity of the fabricated sensor, interference studies were carried out with potentially interfering ions, such as other nitro aromatic compounds and common ions. Fig. 5 depicts the interference currents for 10-fold excesses of paraxon, fenitrothion, nitrobenzene (NB), *p*-nitrophenol (NP), nitroaniline (NA) and 100-fold excesses of Na^+, K^+, Ca^{2+}, PO_4^{3-}, NO_3^-, Cl^- in the presence of a constant concentration of 10 μM MP. From the observed results, the fabricated sensor showed an interference current of less than 5% for other nitro compounds and no significant current changes for the common ions. The present study stated that the NCN modified GCE electrode exhibits selective detection towards MP, endorsing the hired material for practical application.

3.6. Oxygen reduction reaction on NCN modified GCE

To assess the ORR catalytic activity, the NCN modified GCE was subjected to CV in N_2 and O_2 saturated 0.1 M NaOH. Fig. 6a exhibits a strong electrocatalytic oxygen reduction curve for the NCN modified GCE at −0.147 V *vs.* Ag/AgCl in the presence of O_2, which is a low overpotential compared to conventional carbon electrodes.[7] In contrast, the obtained ORR curve is obviously different from its background current in N_2 saturated 0.1 M NaOH, where the NCN modified GCE shows only double layer capacitance behavior. The performance of the NCN modified GCE was compared with the commercially viable and state of the art catalyst, platinum.

Remarkably, the NCN modified GCE reveals only a 130 mV overpotential compared to the commercial Pt/C catalyst and also shows similar electrocatalytic current for the ORR (Fig. 6b). The ORR activity of the NCN modified GCE electrode gives rise to excellent electrocatalytic current compared to previously reported N-doped carbons.[8,15] Moreover, RDE measurements were used to analyze the ORR kinetics of the NCN modified GCE in O_2 saturated 0.1 M NaOH. Fig. 6c depicts the linear sweep

voltammetry (LSV) of the NCN modified GCE at various rotation rates. The NCN modified GCE reveals a one step oxygen reduction with a plateau of steady state diffusion current for all rotations. The kinetic parameters and electron transfer were evaluated by the Koutecky–Levich (KL) equation. Fig. 6d shows the KL plots for the NCN modified GCE, which are linear and parallel which suggested that the obtained ORR follows first-order reaction kinetics with respect to the concentration of dissolved oxygen. In addition, each rotation has an almost identical electron transfer number for the ORR at different potentials. The number (n) of electron transfer was calculated to be ~3.98 to 4.02 from the slopes of the KL plots for the different potentials from 0.45 to 0.65 V. This observed electron transfer number suggested that NCN modified GCE favors a $4e^-$ oxygen reduction process, unlike other carbonaceous materials. Hence, it can be used as an alternative material in fuel cells to the cost effective and rare earth abundant platinum.

3.7. Mechanisms of ORR and MP detection

The NCN modified GCE exhibits a diversity of applications due to its divergent properties, due to the different bonding environments of the nitrogen atoms in the carbon lattice. As mentioned earlier, the nitrogen atoms comprise two major components in NCN; namely, pyrrollic and pyridinic nitrogen (Fig. 1a).

Commonly, pyrrole is known for its electron rich aromatic ring and is basic in nature which provides the grounds for MP adsorption. The nitro group of MP was easily attracted by the C-3 position in pyrrole, because that position is highly electron rich in pyrrole (Scheme 2c). Following the adsorption, the MP was directly reduced to arylhydroxylamine by a proton coupled four electron transfer (PCET) and the as-reduced compound was further oxidized into an arylnitroso group. In contrast, bare GCE also followed the same reaction pathway; however, the aforementioned mechanism provides better understanding about the reaction. In NCN, the pyrrole ring initiates the reaction, and hence the activation energy is reduced; therefore, the NCN modified GCE reduces MP at a low overpotential comparable to bare GCE.

On the other hand, the electron deficient pyridinic carbon furnishes the bonding sites for the dissolved oxygen molecule. The sp^2 character of nitrogen in pyridine provides room for a localized electron, and hence the ortho and para positions of the pyridinic group in NCN attain electropositive character and welcome the oxygen molecule (Scheme 2b). The adsorbed oxygen molecule was further reduced *via* a four electron transfer. Usually un-doped carbons are well known for hydrogen peroxide production (*via* a two electron pathway).[43] The N-doped carbons manifest the four electron transfer by the effective adsorption of oxygen molecules and the electrostatic interaction between the π-orbital and the electrons of the pyridinic nitrogen. This mechanistic study demonstrates how the NCN modified GCE can be employed in a diversity of applications and suggests possible interactions with both MP and oxygen.

4. Conclusions

In summary, we have demonstrated a simple and reliable method to prepare nitrogen doped carbon for energy and sensor applications. In the described method, we follow a flame synthesis to produce nitrogen doped carbon from a nitrogen containing organic aromatic compound, namely, pyrrole. Besides that, many different heteroatom doped carbons have to be synthesized from the aforementioned method by varying the precursor compounds. A meticulous evaluation of the as prepared compound (NCN) uncovers superior electrocatalytic activity towards the detection of MP and ORR. Moreover, the NCN modified GCE exhibits reasonable activity towards the determination of MP, and shows an acceptable level of performance compared to previous reports. Furthermore, the NCN modified GCE reveals superior electrocatalytic activity towards ORR compared to the commercial Pt/C catalyst. Hence, the present study paves the way towards a diversity of applications handled by a single compound and also motivates the use of a metal-free catalyst for practical applications.

Acknowledgements

This project was supported by the National Science Council and the Ministry of Education of Taiwan (Republic of China). Research supported by the King Saud University, Deanship of Scientific Research, College of Science, Research Center. The financial support from the Chung Gung Memorial Hospital through contract no. BMRP 280A to BSL is acknowledged.

References

1 N. S. Lewis and D. G. Nocera, *Proc. Natl. Acad. Sci. U. S. A.*, 2006, **103**, 15729.
2 M. Winter and R. J. Brodd, *Chem. Rev.*, 2004, **104**, 4245.
3 A. A. Gewirth and M. S. Thorum, *Inorg. Chem.*, 2010, **49**, 3557.
4 H. Yang, *Angew. Chem., Int. Ed.*, 2011, **50**, 2674.
5 R. Bashyam and P. Zelenay, *Nature*, 2006, **443**, 63.
6 M. Lefevre, E. Proietti, F. Jaouen and J. P. Dodele, *Science*, 2009, **324**, 71.
7 K. Gong, F. Du, Z. Xia, M. Durstock and L. Dai, *Science*, 2009, **323**, 760.
8 R. Liu, D. Wu, X. Feng and K. Muellen, *Angew. Chem., Int. Ed.*, 2010, **122**, 2619.
9 Y. Liang, Y. Li, H. Wang, J. Zhou, J. Wang, T. Regier and H. Dai, *Nat. Mater.*, 2011, **10**, 780.
10 Y. Liang, H. Wang, J. Zhou, Y. Li, J. Wang, T. Regier and H. Dai, *J. Am. Chem. Soc.*, 2012, **134**, 3517.
11 J. Zhang, C. Guo, L. Zhang and C. M. Li, *Chem. Commun.*, 2013, **49**, 6334.
12 Y. Zhi, Z. Yao, G. Li, G. Fang, H. Nie, Z. Liu, X. Zhou, X. Chen and S. Huang, *ACS Nano*, 2011, **6**, 205.
13 Y. Lijun, S. Jiang, Y. Zhao, L. Zhu, S. Chen, X. Wang, Q. Wu, J. Ma, Y. Ma and Z. Hu, *Angew. Chem., Int. Ed.*, 2011, **123**, 7270.
14 S. Wang, L. Zhang, Z. Xia, A. Roy, D. W. Chang, J. B. Baek and L. Dai, *Angew. Chem., Int. Ed.*, 2012, **51**, 4209.

15 L. Qu, Y. Liu, J. B. Baek and L. Dai, *ACS Nano*, 2010, **4**, 1321.
16 L. H. De Aguiar, G. Moraes, I. M. Avilez, A. E. Altran and C. F. Correa, *Environ. Res.*, 2004, **95**, 224.
17 R. Alvarez, M. P. Honrubia and M. P. Herraez, *Arch. Environ. Contam. Toxicol.*, 1995, **28**, 349.
18 A. Cappielo, G. Famiglini, P. Palma and F. Mangani, *Anal. Chem.*, 2002, **74**, 3547.
19 S. Lacorte and D. Barcelo, *Anal. Chem.*, 1996, **68**, 2464.
20 R. Eiser, K. Levsen and G. Wunsch, *J. Chromatogr. A*, 1996, **733**, 143.
21 C. Li, C. Wang, C. Wang and S. Hu, *Sens. Actuators, B*, 2006, **117**, 166.
22 A. K. Geim and K. S. Novoselov, *Nat. Mater.*, 2007, **6**, 183.
23 M. Taghioskoui, *Mater. Today*, 2009, **12**, 34.
24 L. A. Ponomarenko, F. Schedin, M. I. Katsnelson, R. Yang, E. W. Hill, K. S. Novoselov and A. K. Geim, *Science*, 2008, **320**, 356.
25 H. B. Zhang, J. W. Wang, Q. Yan, W. G. Zheng, C. Chen and Z. Z. Yu, *J. Mater. Chem.*, 2011, **21**, 5392.
26 S. Stankovich, D. A. Dikin, R. D. Piner, K. A. Kohlhaas, A. Kleinhammes, Y. Jia, Y. Wu, S. T. Nguyen and R. S. Ruoff, *Carbon*, 2007, **45**, 1558.
27 L. Wang, Q. Zhang, S. Chen, F. Xu, S. Chen, J. Jia, H. Tan, H. Hou and Y. Song, *Anal. Chem.*, 2014, **86**, 1414.
28 V. Budarin, J. H. Clark, J. J. Hardy, R. Luque, K. Milkowski, S. J. Tavener and A. J. Wilson, *Angew. Chem., Int. Ed.*, 2006, **118**, 3866.
29 H. Zhu, X. Wang, F. Yang and X. Yang, *Adv. Mater.*, 2011, **23**, 2745.
30 J. Wei, D. Zhou, Z. Sun, Y. Deng, Y. Xia and D. Zhao, *Adv. Funct. Mater.*, 2013, **23**, 2322.
31 D. S. Yang, D. Bhattacharjya, S. Inamdar, J. Park and J. S. Yu, *J. Am. Chem. Soc.*, 2012, **134**, 16127.
32 D. Bhattacharjya, H. Y. Park, M. S. Kim, H. S. Choi, S. N. Inamdar and J. S. Yu, *Langmuir*, 2014, **30**, 318.
33 H. Liu, T. Ye and C. Mao, *Angew. Chem., Int. Ed.*, 2007, **46**, 6473.
34 X. Deng, L. Mammen, H. J. Butt and D. Vollmer, *Science*, 2012, **335**, 67.
35 Z. Q. Li, C. J. Lu, Z. P. Xia, Y. Zhou and Z. Luo, *Carbon*, 2007, **45**, 1686.
36 K. Ghosh, M. Kumar, T. Maruyama and Y. Ando, *Carbon*, 2010, **48**, 191.
37 P. Han, Y. Yue, L. Zhang, H. Xu, Z. Liu, K. Zhang, C. Zhang, S. Dong, W. Ma and G. Cui, *Carbon*, 2012, **50**, 1355.
38 Z. S. Wu, W. Ren, L. Xu, F. Li and H. M. Cheng, *ACS Nano*, 2011, **5**, 5463.
39 S. W. Lee, N. Yabuuchi, B. M. Gallant, S. Chen, B. S. Kim, P. T. Hammond and Y. S. Horn, *Nat. Nanotechnol.*, 2010, **5**, 531.
40 G. Liu and Y. Lin, *Anal. Chem.*, 2005, **77**, 5894.
41 D. Du, J. Liu, X. Zhang, X. Cui and Y. Lin, *J. Mater. Chem.*, 2011, **21**, 8032.
42 S. Anandhakumar, K. Dhanalakshmi and J. Mathiyarasu, *Electrochem. Commun.*, 2014, **38**, 15.
43 I. Yamanaka, T. Onizawa, S. Takenaka and K. Otsuka, *Angew. Chem., Int. Ed.*, 2003, **42**, 3653.
44 J. C. Ma and W. D. Zhang, *Microchim. Acta*, 2011, **175**, 309.
45 D. Du, M. Wang, J. Zhang, J. Cai, H. Tu and A. Zhang, *Electrochem. Commun.*, 2008, **10**, 85.
46 S. Xia, J. Zhang and C. Li, *Anal. Bioanal. Chem.*, 2010, **396**, 697.
47 H. Parham and N. Rahbar, *J. Hazard. Mater.*, 2010, **177**, 1077.
48 D. Pan, S. Ma, X. Boa and L. Guo, *Microchim. Acta*, 2011, **173**, 215.
49 Y. Bian, C. Li and H. Li, *Talanta*, 2010, **81**, 1028.
50 Y. Zeng, D. Yu, Y. Yu, T. Zhou and G. Shi, *J. Hazard. Mater.*, 2012, **217**, 315.
51 Y. Li, M. Xu, P. Li, J. Dong and S. Ai, *Anal. Methods*, 2014, **6**, 2157.
52 X. C. Fu, J. Zhang, Y. Y. Tao, J. Wu, C. G. Xie and L. T. Kong, *Electrochim. Acta*, 2015, **153**, 12.
53 R. Thota and V. Ganesh, *Sens. Actuators, B*, 2016, **227**, 169.